VOL. 10, NO. 14, AUGUST 2015 ISSN 1819-6608
ARPN Journal of Engineering and Applied Sciences

www.arpnjournals.com

ROAD RESTRAINT SYSTEMS MONITORING WITH STEREOSCOPIC DIP-TECHNIQUE

Marco Guerrieri[1, 2] and Raffaele Mauro[1]
[1] Department of Civil, Environmental and Mechanical Engineering, University of Trento, Italy
[2]Euro-Mediterranean Institute of Science and Technology (IEMEST), Via Emerico Amari, Palermo, Italy
E-Mail: marco.guerrieri@tin.it

ABSTRACT

Road restraint systems (RRS) are used to protect vehicle occupants from dangerous roadside elements such as rigid obstacles, slopes, utility poles, etc. The crashes on a road restraint system damage its structure and, therefore, the functional behavioral; for this reason is required monitoring the RRS into their operational conditions. The research addresses the problem of the measurement of safety barrier (SB) deformations by means digital image processing technique (DIP). This technique is founded on the analysis of high resolution photos/videos, obtained by means of 3D camera installed into a data vehicle. The DIP technique has been used for evaluating the longitudinal safety barriers deformations. A case study concerning N2 W-beam guardrails installed along a rural road in Italy was examined. The procedure has shown that the DIP technique can be used with the aim to monitoring guardrails and, therefore, to identify the cases in which damaged SB must be repaired or replaced.

Keywords: road restraint systems (RRS), w-beam guardrail, digital image processing (DIP), stereoscopic

INTRODUCTION

Road restraint systems (RRS) - safety barriers, crash cushions, terminal of barriers, transitions among different road restraint systems, motorcyclist protection devices - are used to protect vehicle occupants from dangerous roadside elements such as rigid obstacles, slopes, utility poles and other dangerous obstacles [1].

Safety barriers (SB) are currently designed for different performance levels, which are set according to current CEN performance standards [2] using three main criteria:

- vehicle containment;
- impact severity to occupants;
- deformation width of the barrier.

In Europe, the safety barriers are classified in the following main types: N1, N2, H1, H2, H3, H4a and H4b (cfr. Figure-1), as function of the containment Level (CL). It indicates the barrier's strength, by specifying the maximum amount of kinetic energy the barrier is able to contain.

According to EN 1317 [2] there are three different containment levels: T - low containment level (T1-T3), N - normal containment level (N1-N2), and H – high (H1-H3) or very high containment level (H4a-H4b). The values of CL associated with each safety barrier type are shown in Table-1.

For each of the previous types, a standard crash test is assumed to be representative of real accidents (speed and angle of crash are given by line guide).

However, the cinematic of real accidents rarely are very similar to the impact conditions as simulated in the crash test.

For evaluating the injury risk in the event of a motor vehicle crash test, two different type of criteria has been developed:

- Anthropometric test device based injury criteria (i.e. Abbreviated Injury Scale (AIS), Head Injury Criterion (HIC));
- Vehicle-based injury criteria (Acceleration Severity Index (ASI), Theoretical Head Impact Velocity (THIV), Post-impact Head Deceleration (PHD)).

There are many reasons why vehicles leave the pavement and encroach onto the roadside, including: driver fatigue or inattention, excessive speed, driving under the influence of drugs or alcohol, crash avoidance, rebound off an initial crash within the roadway, environmental condition such as ice, rain or poor visibility, vehicle component failure.

Roque and Cardoso [1] show that for predicting roadside crash frequency (crashes on a roadway section during a prefixed time period) can be used the Poisson and the negative binomial regression count models, as follows:

- **Poisson regression**

$$P(y_{ij}) = \frac{e^{-\lambda_{ij}} \cdot \lambda_{ij}^{y_{ij}}}{y_{ij}!} \quad (1)$$

Where $P(y_{ij})$ is the probability of y crashes occurring on highway element i during time period j and λ_{ij} is the expected value of y_{ij},

$$E(y_{ij}) = \lambda_{ij} = e^{\beta X_{ij}} \quad (2)$$

For a roadway section i in time period j, β is the vector of parameters to be estimated and X_{ij} is a vector of explanatory variables describing roadway section geometric characteristics, environmental characteristics and other relevant roadside features that may affect crash frequency, such as traffic.

- **Negative binomial model**

The negative binomial model is derived by rewriting Poisson parameter for each observation i in a given time interval j as [3]:

$$\lambda_{ij} = e^{(X\beta_{ij}+\varepsilon_{ij})} \quad (3)$$

where $\exp(\varepsilon_{ij})$ is a random error term that follows a Gamma probability distribution with mean 1 and variance α. This addition allows the variance to differ from the mean as stated below:

$$VAR[y_i] = E[y_i]\cdot(1+\alpha\cdot E[y_i]) = E[y_i] + \alpha E[y_i]^2 \quad (4)$$

The national and local road authorities take limited funding for addressing guardrails need for new installations and for change existing damage barriers or sub-standards guardrails.

Generally, for good allocations of the funding, cost-effectiveness analysis (CEA) are carried out.

CEA are based on the evaluation of roadside safety improvements using encroachment probability models and accident-data.

The principal aim is to maximize the total length of hazardous site protection for given monetary budget. For this propose Roadside Safety Analysis Program software (RSAP) can be used [4].

The annual crash probability can be estimated according to the Cooper study [5]. In addition, this study is implemented in the RSAP [4, 5].

RASP is based on the assumption that crash frequency is proportional to encroachment frequency, which is a function of the highway type or functional class and average daily traffic (Figure-2).

The probability $P(C_{v\psi}^{w\theta} / E_{v\psi}^{w\theta})$ that a vehicle (of size w, encroaching with a given speed v, angle θ, and orientation ψ) is within the hazard envelope and encroaching far enough to impact the hazard is given by the following relation [4]:

$$P(C_{v\psi}^{w\theta} / E_{v\psi}^{w\theta}) = (1/5280)\cdot[L_h \cdot P(L_e \geq A) + \sec\theta\cdot\csc\theta\cdot\sum_{j=1}^{We\cos\theta} W_e P(L_e \geq B) + \cot\theta\cdot\sum_{j=1}^{W_h} P(L_e \geq C)] \quad (5)$$

The probability of an impact on the safety barrier $P(C/E)$ can be obtained by means eq. (6):

$$P(C/E) = \sum_w\sum_v\sum_\theta\sum_\psi P(E_{v\psi}^{w\theta}/E)\cdot(C_{v\psi}^{w\theta}/E_{v\psi}^{w\theta}) \quad (6)$$

Where $P(C/E)$ is the probability of a crash "C" given an encroachment "E". $P(C_{v\psi}^{w\theta}/E)$ is the probability of an encroachment with a given vehicle type *w*, speed *v*, angle θ, and vehicle orientation ψ.

L_h, L_e, A, W_e, B, j, C are the geometric parameters used to describe the encroachment path [4, 5].

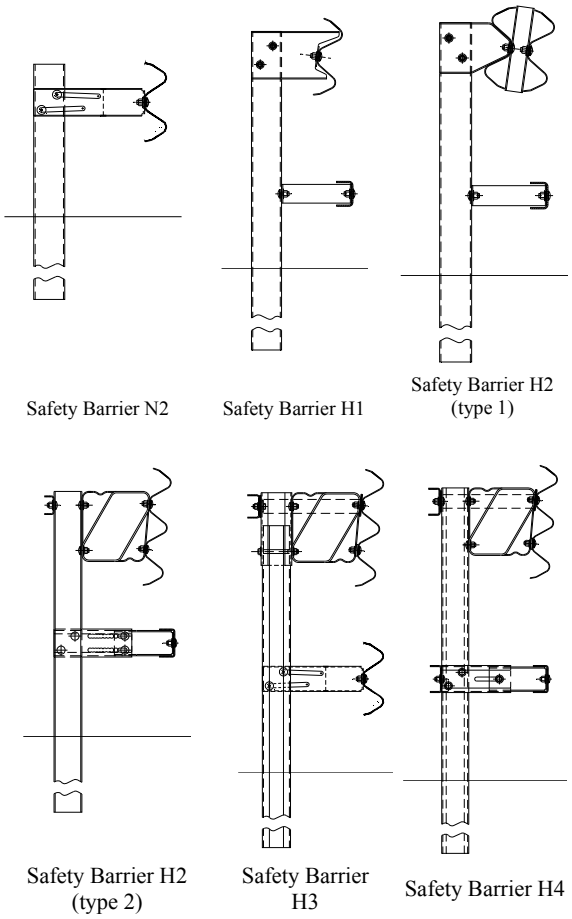

Figure-1. Safety barriers types.

Table-1. Conteiment level of safety barriers.

Safety barrier type	**Containment level** (CL) [kJ]
N1	44
N2	82
H1	127
H2	288
H3	463
H4a	572
H4b	724

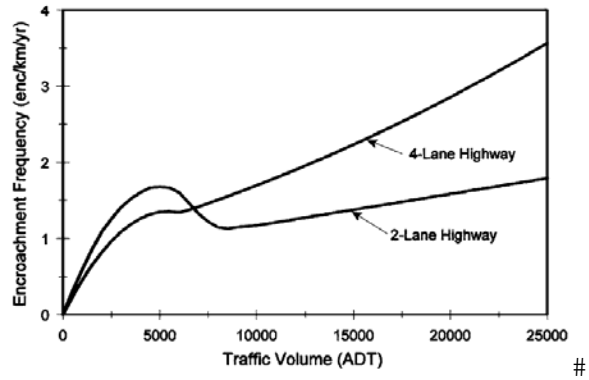

Figure-2. Encroachment frequency as function of traffic volume (source [5]).

The main scaling procedures used to characterize the severity of injury and the probability of death from multiple injuries, are the Abbreviated injury scale (AIS) and the Injury severity score (ISS) [6].

For the crashes against the safety barriers are of interest the injury measures concerns the head impact due to the potential severe consequences. The Head injury criterion (HIC) is computed as [7]:

$$HIC = \max\left[\frac{1}{t_2 - t_1}\int_{t_1}^{t_2} a(t)dt\right]^{2,5}(t_2 - t_1) \quad (7)$$

where t_1 and t_2 are arbitrary times within the acceleration pulse. Acceleration, a(t), is expressed as a multiple of gravitational acceleration ($g = 9{,}8\ m/s^2$).

The Head injury criterion is used, as example, to pass the test of the Federal Motor Vehicle Safety Standard (FMVSS 208) successfully [8]. In USA, the automobile manufacturers must demonstrate, when subjected to a 30 mph frontal barrier impact that a fully restrained 50th percentile male Anthropomorphic Test Device (ATD) is exposed to HIC scores of less than 700 and 1000, evaluated over maximum time intervals of 15 ms and 36 ms, respectively [8].

The Head impact power (HIP) is used as a criterion for evaluating the mild traumatic brain injury (MTBI), defined as "*a trauma induced alteration in mental status that may or may not involve loss of consciousness*" [9].

The HIP is used to measure the change in translational and in rotational kinetic energy of the head [10, 11, 12]:

$$\text{Power} = P = \sum ma \cdot v + \sum I\alpha \cdot \omega \quad [kW] \quad (8)$$

Where: m is the mass of the head; I is the rotational inertia, a is the linear acceleration; v is the linear velocity; α is the angular acceleration, and ω is the angular velocity.
When the coefficients are set equal to the mass and appropriate mass moments of inertia for the human head, the expression becomes:

$$HIP = 4{,}50a_x\int a_x dt + 4{,}50a_y\int a_y dt + 4{,}50a_z\int a_z dt + 0{,}016\alpha_x\int \alpha_x dt + 0{,}024\alpha_y\int \alpha_y dt + 0{,}022\alpha_z\int \alpha_z dt \quad (9)$$

The Figure-3 shows the correlation between the probability of concussion and the maximum value of the Power Index (HPI_m) [10].

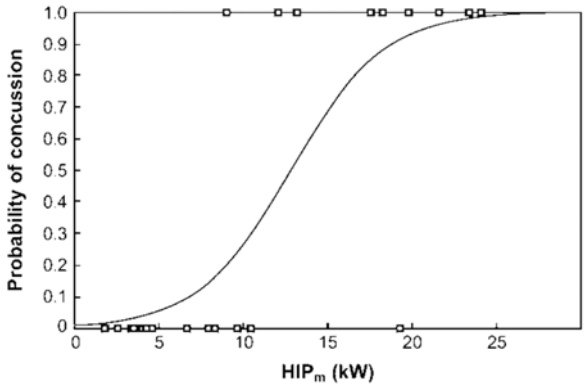

Figure-3. Probability of concussion as function of the maximum value of the Power Index (source [6]).

The crashes on the barrier damage its structure and the functional behavioral (in fact the w-beam absorbs the kinetic energy of the impacting vehicle by means of plastic deformations) for this reason is required monitoring the guardrails into their operational conditions [13, 14].

Image processing technique offers great potentialities in highway and in railway engineering [15, 16, 17], so the technique based on digital image analysis, (DIP) can be used for evaluation the longitudinal barriers deformations in a precise and quick way [18].

THEORY

In the present research, we applied DIP technique with the stereoscopic method. The acquisition system used for the dataset of our experiments consists into a 3D-Camera (Samsung NX 300 camera system, equipped with a 45mm f/1.8, 2D/3D lent) that was installed into a data vehicle by means a telescopic arm. The photos have been taken with a car speed between 20 to 30 km/h.

Due to the relative speed between objects (guardrails) and data vehicle, the planar surface under perspective projection can be described as a second order function of image coordinates involving eight independent parameters. Therefore, the image motion induced by a rigidly moving object can be obtained as in [19, 20, 21, 22]:

$$u(x) = \frac{1}{Z(x)} A(x)t + B(x)\omega \quad (10)$$

Where Z(x) is the distance from the camera of the point whose image position is x = (x, y), and

$$A(x) = \begin{bmatrix} -f & 0 & x \\ 0 & -f & y \end{bmatrix} \quad (11)$$

$$B(x) = \begin{bmatrix} (xy)/f & -(f^2 + x^2)/f & y \\ (f^2 + x^2)/f & -(xy)/f & -x \end{bmatrix} \quad (12)$$

The A and the B matrices depend only on the image positions and the focal length f of the camera. Also, t is the translation vector and ω the angular velocity vector. Substituting into eq. (10) the eq. (11) and eq. (12) we obtain:

$$u(x) = [A(x)t] \cdot [r(t)^T K] + B(x)\omega \quad (13)$$

This flow field is quadratic in (x) and can be written as:

$$u(x) = a_1 + a_2 x + a_3 y + a_7 x^2 + a_8 xy \quad (14)$$

$$v(x) = a_4 + a_5 x + a_6 y + a_7 xy + a_8 y^2 \quad (15)$$

Where the 8 coefficients a_i, i=1, 2,3…8 are functions of the motion parameters t, ω and the surface parameters K. Since this 8-parameter form is rather well-known [23, 24, 25, 26] we omit its details.

In the case of Stereoscopy (based on the analysis of images coming from two video cameras located at a certain distance between each other, called baseline) the most general form of the perspective projection matrix can be written as follows:

$$\tilde{P}_{new} = C \cdot [I|0] \cdot G = C \cdot [R|T] \quad (16)$$

Where:

$$C = \begin{bmatrix} f \cdot k_u & 0 & u_0 \\ 0 & f \cdot k_v & v_0 \\ 0 & 0 & 1 \end{bmatrix} \quad (17)$$

While R and T are respectively the translation vector and the rotation vector derived from the preliminary calibration procedure.

$$R = \begin{bmatrix} r_1^T \\ r_2^T \\ r_3^T \end{bmatrix} \quad (18)$$

$$T = \begin{bmatrix} t_1 \\ t_2 \\ t_3 \end{bmatrix} \quad (19)$$

Matrix C encodes the intrinsic parameters (f, k_u, k_v,u_0, v_0) of the video camera, on the other hand matrix G encodes the extrinsic parameters (R and T [18]). The $\tilde{P}_{new}$ represents the Perspective Projection Matrix (PPM) which regulates the projection of space points (referred to the system-world) onto the image plane. In the case under examination (cfr. next section), downstream of the rectification procedure, the two perspective transformed images have been determined and the image pairs generating the 3D have been rectified.

Figure-4. Left and right barrier images rectified

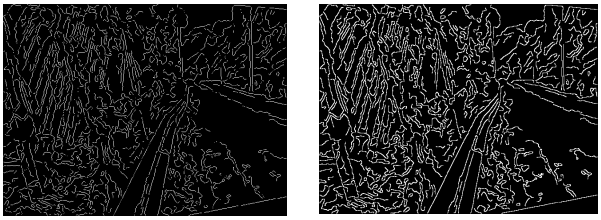

Figure-5. Binary image (Canny algorithm [22])

Figure-6. Binary image without discontinuity

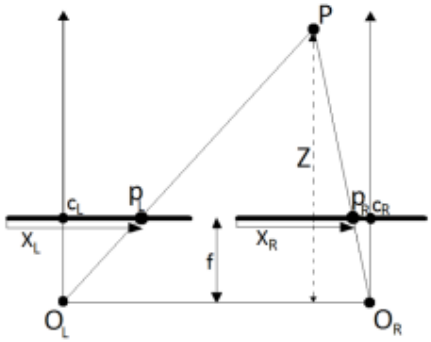

Figure-7. Stereo system.

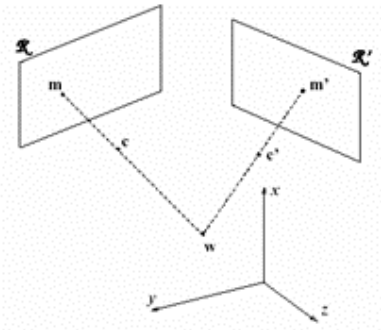

Figure-8. Axonometric projection of the conjugate points in the stereoscopic triangulation process.

The main problem to be faced in the 3D construction is the correspondence that is the search for the projection of the same physical point onto both images (matching point search). This problem is handled with global or local methods. The correct and rapid correspondence estimation is mathematically and computationally complex. The main difficulties which may lead to an erroneous association of two non-corresponding points are due to: occlusions, distortions, different camera parameters, specular reflections, sensor noise.

The possibility of detecting an object distance is extremely important in this research. Indeed, only a tridimensional analysis of the safety barrier dominion in its real form and dimension may lead to inferences about its functional efficiency state.

The simplest case of 3D search occurs in presence of a canonical stereo system, that is when the corresponding images have no distortions and are perfectly coplanar and aligned by pixel line, with perfectly parallel axes, coinciding focal lengths and so calibrated main points cL and c_R that are at the same pixel coordinates in both images. Such an array, called fronto-parallel, is shown in Figure-7 [27].

As previously mentioned, the straight line connecting the optical centers O_L and O_R of the two video cameras is called baseline. By means of a simple geometrical analysis of Figure-7, depth Z is deduced as inversely proportional to the disparity $X_L - X_R$.

The stereo-triangulation (cfr. Figure-8) is the methodology which allows to evaluate the 3D point place in the space starting from the pixel coordinates of its projections onto the retinal sensor planes.

Given the perspective projection matrices, which regulate the projection of a coordinate point w (see Figure-8) onto the two image planes, and given the homogeneous pixel coordinates of its projections, the w position can be obtained by intersecting optical rays associated to the planes. The following relations give the position of a generic point in the space-world:

$$\begin{cases} w = c_1 + \lambda_1 + (A_n \cdot R_n)^{-1} \cdot \tilde{m}_{n1} \\ w = c_2 + \lambda_2 + (A_n \cdot R_n)^{-1} \cdot \tilde{m}_{n2} \end{cases} \quad (20)$$

Where A_n and R_n are the new matrices resulting from the rectification and the coordinates and are the new w projections onto the retinal planes after the rectifying transformations and the compensation for radial and tangential distortions. The coordinates of a generic point in the world, can be denoted as follows [12]:

$$w_{left} = \begin{bmatrix} x_1 \\ y_1 \\ z_1 \end{bmatrix} \quad (21)$$

$$w_{right} = \begin{bmatrix} x_2 \\ y_2 \\ z_2 \end{bmatrix} \quad (22)$$

$$\hat{w} = \frac{w_{left} + w_{right}}{2} \quad (23)$$

CASE STUSY AND RESULTS

The DIP technique has been applied for evaluation the damage of W- beam N2 guardrail (cfr. Figure-1 and Figure-4) installed along one rural road in Italy (road SS 117 bis in Sicily).

The transversal and vertical distortions of guardrails have been carried out by means of the 3D analysis. The Figures 10-15 show the diagrams of guardrails' deformation for three sections of the road SS 117 bis (sections n. 1, 2 and 3) obtained with the projection of the 3D model of the longitudinal barrier (see Figure-4 and Figure-9) onto the plan (XY) and (XZ). The longitudinal

distance Δ between the section 1 and 2 and between the section 2 and 3 is equal to 5 m.

For the guardrail under analysis, the maximum transversal deformation Y is 17, 8 cm, instead the maximum value of vertical deformation is 7, 5 cm.

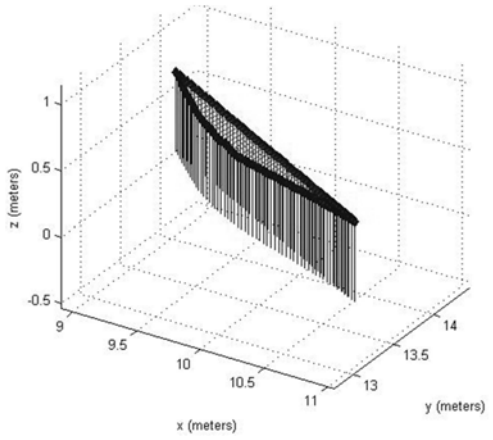

Figure-9. 3D Model: deformed barrier in comparison with the original configuration.

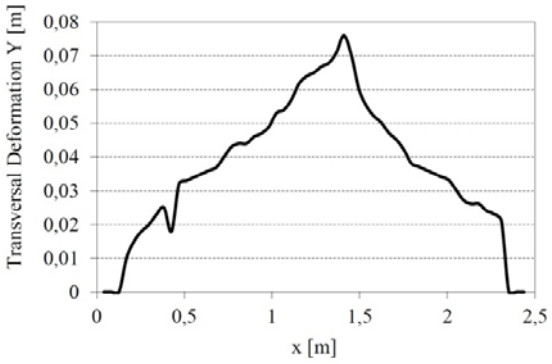

Figure-10. Deformation on the plane XY (section 1).

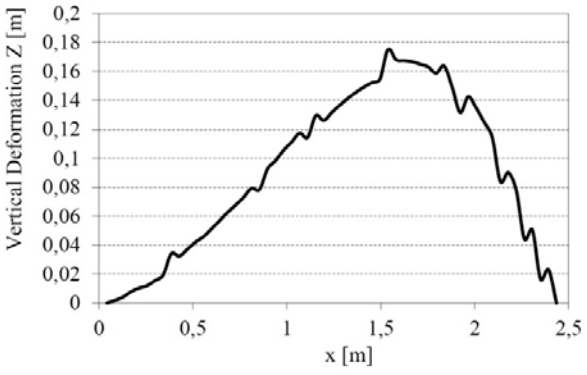

Figure-11. Deformation on the plane XZ (section 1).

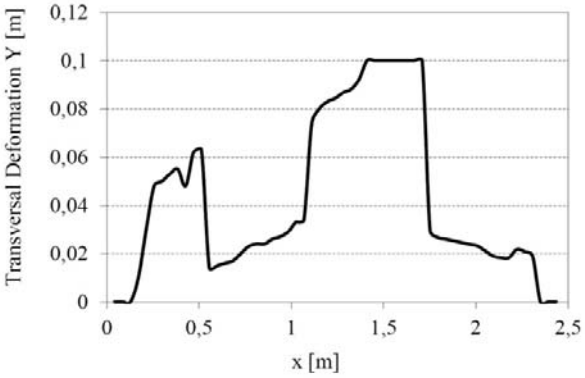

Figure-12. Deformation on the plane XY (section 2).

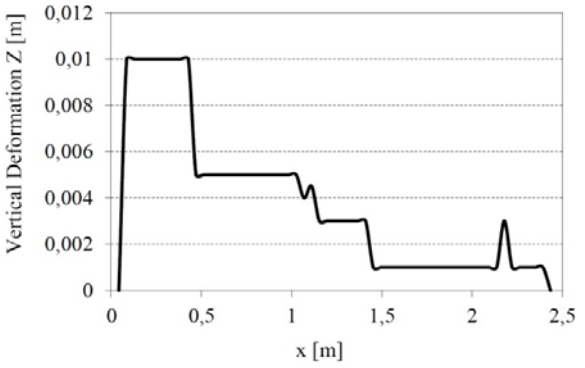

Figure-13. Deformation on the plane XZ (section 2).

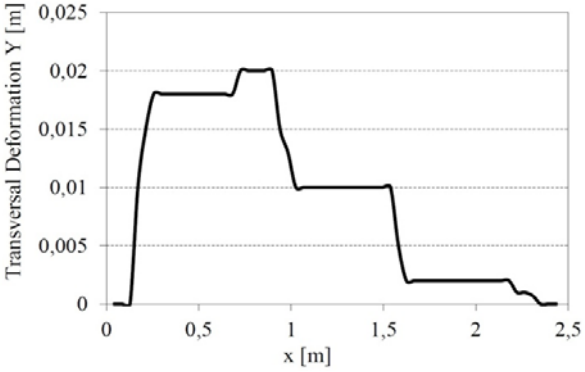

Figure-14. Deformation on the plane XY (section 3).

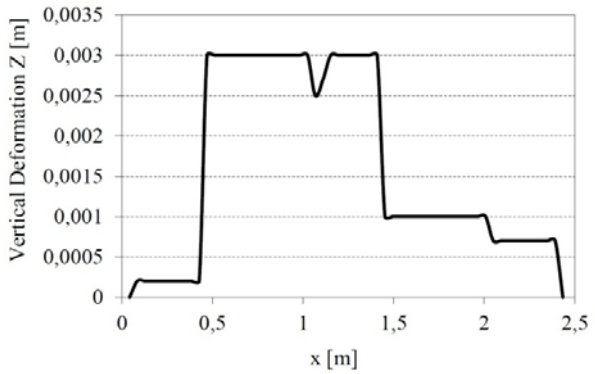

Figure-15. Deformation on the plane XZ (section 3).

CONCLUSIONS

The crashes on the road restraint systems (RRS) (specially the safety barriers) can damage their structures. The results of this paper explain the potentiality offered by digital image technique (DIP) for the measurement of longitudinal safety barriers (SB) deformations, due to vehicles crashes. With the use of a 3D-Camera (Samsung NX 300 camera system, equipped with a 45mm f/1.8 2D/3D lent), installed into a data vehicle, have been done many experimental measurement of an N2 W-beam safety barrier along an Italian rural road (SS 117 bis in Sicily, Italy). The images of the barriers have been analyzed using DIP technique with the stereoscopy method. The procedure developed in the research shows how the DIP method allows evaluating the transversal (XZ plan) and vertical deformations (XZ plan) of the guardrails in a very precise and rapid way. So, with the aim to guarantee reasonable road safety levels, the DIP technique could be used for monitoring the longitudinal safety barriers to identify the cases in which barriers must be repaired or replaced with new SB.

ACKNOWLEDGEMENTS

This work was carried out within the research project “RE.S.E.T. Rete di laboratori per la Sicurezza, Sostenibilità ed Efficenza dei Trasporti della Regione Siciliana”, which is funded from the PO-FESR Sicilia 2007- 2013- Asse IV, Obiettivo operativo 4.1.2, Linea d’intervento 4.1.2.A.

REFERENCES

[1] Roque C, Cardoso J.L. 2013. Observations on the relationship between European standards for safety barrier impact severity and the degree of injury sustained. IATSS Research. 37: 21-29.

[2] 2007. European Committee for Standardization, N 1317-2 road restraint systems-part 2. Technical Committee CEN/TC 226, Brussels.

[3] Karlaftis Washington M, Mannering F.L. 2011. Statistical and Econometric Methods for Transportation Data Analysis, Second edition Chapman and Hall/CRC978-1-4200-8285-2.

[4] 2003. Roadside Safety Analysis Program. Engineer’s Manual. NCHRP REPORT 492, TRB, D.C.

[5] Cooper P. 1980. Analysis of Roadside Encroachments Single Vehicle Run-off-Road Accident Data Analysis for Five Provinces. B. C. Research, Vancouver, British Columbia, Canada.

[6] Hayes W. C., Erickson M. S., Power E. D. 2007. Forensic Injury Biomechanics. Annu. Rev. Biomed. Eng. 9: 55-86.

[7] Kleinberger M., Sun E., Eppinger R., Kuppa S., Saul R. 1998. Development of improved injury criteria for the assessment of advanced automotive restraint systems. NHTSA. Doc. 98-4405-9.

[8] 2005. NHTSA. Federal Motor Vehicle Safety Standards: Occupant crash protection, FMVSS 571.208, Stand. No. 208, pp. 567-653.

[9] 1997. Quality Stand. Subcomm. Practice parameter: the management of concussion in sports. Neurology. 48, 581-85.

[10] Newman J. A., Shewchenko N., Welbourne E. A. 2000. Proposed New Biomechanical Head Injury Assessment Function - The Maximum Power Index. 44th Stapp Car Crash Conference Atlanta, Georgia.

[11] Schmitt K.U., Niederer P., Muser M., Walz F. 2010. Trauma Biomechanics, Accidental Injury in Traffic and Sports. Third Edition. Springer.

[12] Shojaati M. 2003. Correlation between injury risk and impact severity index ASI. 3rd Swiss Transport Research Conference, Ascona.

[13] Martin J.-L., Mintsa-Eya C., Goubel C. 2013. Long-term analysis of the impact of longitudinal barriers on motorway safety. Accident Analysis and Prevention. 59, 443-451.

[14] La Torre F., Domenichini L., Meocci M., Nocentini A., Morano S.G. 2015. Evaluation of the vehicle/safety barrier/sign support interaction by means of FEM simulations. International Journal of Crashworthiness. 20(2): 123-133.

[15] Guerrieri M., Corriere F., Parla G., Ticali D. 2013. Estimation of pollutant emissions from road traffic by image processing techniques: A case study in a suburban area. ARPN Journal of Engineering and Applied Sciences. 8(8): 668-676.

[16] Guerrieri M., Ticali D. 2011. Design standards for converting unused railway lines into greenways. Proceedings of the International Conference on Sustainable Design and Construction. 2012, 654-660.

[17] Guerrieri M., Parla G. 2013. A new high-efficiency procedure for aggregate gradation determination of the railway ballast by means image recognition method. Archives of Civil Engineering. 59(4): 469-482.

[18] Guerrieri M., Parla G., Corriere F. 2013. A new methodology to estimate deformation of longitudinal safety barriers. ARPN Journal of Engineering and Applied Sciences. 8(9): 763-769.

[19] Richards J.A. 2013. Remote Sensing Digital Image Analysis. Fifth Edition.

[20] Fernandez-Maloigne C. 2013. Advanced Color Image Processing and Analysis.

[21] Mitiche A., Aggarwal J.K. 2014. Computer Vision Analysis of Image Motion by Variational Methods.

[22] Canny J. 1986. A Computational Approach to Edge Detection. IEEE T Pattern Anal. 8(6): 679-698.

[23] Horn B. K. P. 1986. Robot Vision. MIT Press, Cambridge, MA.

[24] Hartley R., Zisserman A. 2003. Multiple View Geometry in Computer Vision, 2nd edition. Cambridge University Press.

[25] Hartley R., Zisserman A. 2000. Multiple View geometry in Computer Vision. Cambridge University Press.

[26] Faugeras O. 1993. Three-Dimentional Computer Vision. MIT Press, Cambridge, MA. 33-68.

[27] Zhang Z. 1998. Determining the epipolar geometry and its uncertainty: A review. International Journal of Computer Vision. 27(2): 161-195.